Electronic Supplementary Material (ESI) for Soft Matter.

Electronic Supporting Information

Divergent Self-Assembly Propensity of Enantiomeric Phenylalanine Amphiphiles that Undergo pH-Induced Nanofiber-to-Nanoglobule Conversion

Manas Kumar Pradhan, Nayanika Misra, Fathima Sahala, Nyaya Prakash Pradhan, Aasheesh Srivastava*

Department of Chemistry, IISER Bhopal, Bhopal 462066, Madhya Pradesh India.

Email: asrivastava@iiserb.ac.in Homepage: *https://sites.google.com/iiserb.ac.in/aslab/home*

Contents

1.0 Experimental Section

1.1 Materials

All the chemicals mentioned were procured from commercial sources and were of the highest purity available. L-Phenylalanine (F), 1-Naphthylacetic acid (NAA), 1,1-Carbonyldiimidazole (CDI), and ethylenediamine (EDA) were purchased from Spectrochem and used without further purification. Solvents used in the synthesis were further purified, dried, or distilled, as required. Milli-Q water was used during the synthesis. Nuclear Magnetic Resonance (NMR) spectra were recorded on Bruker's AVANCE-III (500 MHz) spectrometers using D_2O, $CDCl_3$, and DMSO-d_6 as solvents, and the chemical shifts are reported in ppm. High-Resolution Mass Spectrometry (HRMS) was recorded by electrospray ionization (ESI) mode using Agilent LCQTOF instrument.

1.2 Representative Synthesis of L/D-NapF-EDA

200 mg L-NapF-OMe (synthesis and characterization of NapF-OMe was reported in our previous publication)[1] (1 eq.,0.58 mmol) was dissolved in EtOH (3 mL). In another RB dry ethylenediamine (200 µL, 1.44 mmol) was dissolved in EtOH (1 mL). L-NapF-OMe solution was added dropwise to the amine solution with stirring. After addition reaction was brought to reflux. The reaction was monitored by TLC. The complete consumption of starting material was observed after 36 h. Ethanol was removed by a rotary evaporator. The product was extracted by workup with $CHCl_3$ and $NaHCO_3$ solution. The chloroform layer was dried over anhyd. sodium sulfate. Chloroform was removed by rotary evaporator; the obtained solid was washed with diethyl ether and pentane. This resulted in an off-white solid with a 70 % yield (see Fig. S1).

^{1}H NMR of **L-NapF-EDA** (500 MHz, $CDCl_3$) δ 7.81 (s, 2H), 7.76 (d, J = 8.3 Hz, 1H), 7.47 – 7.41 (m, 2H), 7.36 (t, J = 7.4 Hz, 1H), 7.26 (d, J = 6.6 Hz, 1H), 7.03 (d, J = 7.2 Hz, 3H), 6.77 (d, J = 6.6 Hz, 2H), 5.98 (s, 1H), 5.85 (d, J = 6.6 Hz, 1H), 4.50 (d, J = 7.1 Hz, 1H), 3.92 (s, 2H), 3.03 (d, J = 5.5 Hz, 2H), 2.85 (dd, J = 13.6, 6.5 Hz, 1H), 2.71 (dd, J = 13.6, 7.0 Hz, 1H), 2.56 – 2.45 (m, 2H).

^{1}H NMR of **D-NapF-EDA** (500 MHz, $CDCl_3$) δ 7.82 (m, 6.4, 3.7 Hz, 2H), 7.76 (d, J = 8.3 Hz, 1H), 7.47 – 7.42 (m, 2H), 7.37 (dd, J = 8.2, 7.1 Hz, 1H), 7.26 (d, J = 7.3 Hz, 1H), 7.07 – 7.01 (m, 3H), 6.80 – 6.76 (m, 2H), 5.96 (s, 1H), 5.85 (d, J = 7.6 Hz, 1H), 4.50 (dd, J = 14.4, 7.2 Hz, 1H), 3.92 (s, 2H), 3.02 (q, J = 5.9 Hz, 2H), 2.88 – 2.81 (m, 1H), 2.71 (dd, J = 13.6, 7.1 Hz, 1H), 2.50 (m, 2H). HR-LCMS: m/z calculated for $C_{23}H_{25}N_3O_2$ $[M+H^+]$ is 376.19; found: 376.20.

1.3 Transmission Electron Microscopy (TEM)

For TEM, samples were prepared on Formvar/carbon film-coated 400 mesh copper grids (Ted Pella). Before adding the sample, the grid was stained using 0.3 w/v% phosphotungstic acid for 20 seconds. Then 10µl of self-assemblies (0.3 mM) was dropped on the grid and left for 120 s and the excess material was bloated out. The grid was dried inside a vacuum desiccator at RT for 12 h. TEM images were recorded after completed drying the samples.

1.4 Rheology

For the strain sweep experiments, a 25 mm diameter, 1° angle cone was used at the top and a flat plate was used at the bottom. The samples were placed on the bottom plate. A 0.05 mm

gap distance was maintained between the cone plate and the flat plate. All the rheological studies were performed at 298 K on the hydrogel (3 mg/mL). Strain sweep tests were performed from 1% to 100% strain at a constant frequency of 10 rad·s^{-1}. Variable temperature (VT) rheological studies were also done at constant amplitude (1% strain) and frequency (10 rad·s^{-1}).

1.5 Determination of the Gel Melting Point

The gel melting point was determined by the "inverse flow method". Hydrogels were prepared in two separate glass vials at the concentration of 3 mg·mL^{-1}, 8 mM of each enantiomer. The vials were inverted and a thermometer was attached to them for recording the temperature. This assembly was immersed inside a water bath with stirring on a hot plate at ambient temperature (298 K). The temperature of the water bath was increased at *ca.* 5 °C·min^{-1}. The temperature range at which the first and last drop of gel mass fell was recorded as the gel melting range temperature.

1.6 Investigation into pH responsiveness

To investigate the effect of pH on the nanostructures formed by the self-assembly of L-NapF-EDA (0.3 mg·mL^{-1}, 0.8 mM), soluble self-assemblies were prepared in five different vials. The pH of the respective solution was adjusted to 5, 6, 7, 8, and 9 by the addition of HCl (1 N) and NaOH (1 N). Optical properties and morphology were studied using CD and TEM.

1.7 pH-dependent reversibility

To investigate the pH-dependent reversibility of enantiomeric self-assembly, 1.5 mg/mL (4 mM) of L-NapF-EDA was used for the hydrogelation. The pH of the gel (inherent pH ~ 8) was reduced to acidic (~ 6) by adding dil. HCl, which led to degradation of gel to sol. After 30 min, pH of the sol was again increased to basic (~8), which allowed the sol to reassemble. The turbidity of the sol also increased after pH adjustment to ~ 8. Digital photos were taken in each step of the reversibility. Diluted the samples to 0.8 mM and recorded the TEM data.

1.8 Tyndall effect

For tyndall effect, self-assembly were prepared at concentration 0.3 mg/mL (0.8 mM) for both the L- and D-NapF-EDA enantiomers. Absorbance was recorded at wavelength range 400-800 nm at a constant temperature 25 °C.

1.9 Data fitting

Temperature-dependent experimental data was fitted in isodesmic model which was previously established by Meijer and coworkers.[2] All heating curves obtained are studied at a slow heating rate of 1.0 K·min^{-1} to ensure the self-assembly processes were under thermodynamic control.

1.10 Computational studies

The structure of L- and D-NapF-EDA were optimized using Gaussian 09[5] software using the following parameters.

Basis set = B3LYP

Level of theory = 6-311++G(d,p)

Charge = 0

Multiplicity = 1

D-NapF-EDA

Symbol	X	Y	Z
C1	-2.6334	1.589726	-1.97458
C2	-2.57208	1.138903	-0.67728
C3	-2.98988	-0.17568	-0.3314
C4	-3.47472	-1.02476	-1.38173
C5	-3.52737	-0.52533	-2.70965
C6	-3.11788	0.751856	-3.00358
H7	-2.29894	2.59346	-2.21032
H8	-2.18032	1.797075	0.087417
C9	-2.94752	-0.68308	1.009094
C10	-3.89367	-2.34459	-1.07635
H11	-3.89643	-1.17799	-3.49408
H12	-3.16049	1.118681	-4.02295
C13	-3.84273	-2.81035	0.213327
C14	-3.37342	-1.97451	1.249156
H15	-4.25518	-2.97814	-1.87945
H16	-4.16589	-3.81883	0.445629
H17	-3.35174	-2.35721	2.264605
C18	-2.46372	0.152921	2.173497
H19	-2.76415	1.199469	2.066279
H20	-2.93512	-0.19416	3.094825
C21	-0.95949	0.170577	2.490523
O22	-0.56746	0.541621	3.591927
N23	-0.11223	-0.21579	1.506975
H24	-0.45466	-0.57395	0.622869
C25	1.318491	-0.31084	1.714688
H26	1.492101	-0.80548	2.677662
C27	2.02549	1.077145	1.811478
H28	3.101936	0.904627	1.915069
H29	1.683498	1.523311	2.746246
C30	1.765743	2.034929	0.67079
C31	0.825054	3.060693	0.817261
C32	2.459005	1.938766	-0.54137
C33	0.580611	3.962721	-0.21706

H34	0.290471	3.15925	1.756531
C35	2.215771	2.83591	-1.57897
H36	3.201646	1.159268	-0.67468
C37	1.274277	3.851655	-1.42049
H38	-0.14502	4.75712	-0.07906
H39	2.765044	2.745086	-2.50965
H40	1.089522	4.554658	-2.22511
C41	1.88011	-1.21381	0.60199
O42	1.216976	-1.51986	-0.37769
N43	3.152496	-1.65363	0.798707
H44	3.628279	-1.38788	1.646312
C45	3.824091	-2.55936	-0.13038
H46	4.559007	-3.13569	0.439011
H47	3.088593	-3.25754	-0.53141
C48	4.512498	-1.83388	-1.29375
H49	5.162644	-1.04092	-0.89122
H50	3.743277	-1.34934	-1.89897
N51	5.214043	-2.80741	-2.13246
H52	5.422984	-2.42852	-3.04833
H53	6.091023	-3.10024	-1.71501

Item	Value	Threshold	Converged ?
Maximum Force	0.000004	0.00045	YES
RMS Force	0.000001	0.0003	YES
Maximum Displacement	0.000401	0.0018	YES
RMS Displacement	0.000097	0.0012	YES

L-NapF-EDA

Symbol	X	Y	Z
C1	-2.8274	0.820876	2.826862
C2	-2.42396	-0.24434	2.05731
C3	-3.13323	-0.62768	0.884937
C4	-4.29436	0.139451	0.529389
C5	-4.68438	1.232729	1.348004
C6	-3.97065	1.570478	2.4712
H7	-2.26308	1.088263	3.713057
H8	-1.54468	-0.79625	2.363511
C9	-2.75429	-1.73038	0.051452
C10	-5.03337	-0.20429	-0.63088
H11	-5.56608	1.799743	1.067079
H12	-4.28079	2.407563	3.08643
C13	-4.6479	-1.26444	-1.41256
C14	-3.51057	-2.02397	-1.06591
H15	-5.90839	0.383556	-0.88779
H16	-5.21455	-1.52733	-2.29874
H17	-3.21444	-2.8545	-1.69703
C18	-1.53241	-2.58781	0.339656
H19	-1.2115	-2.4972	1.377416
H20	-1.7805	-3.63598	0.165915
C21	-0.37342	-2.27059	-0.61264
O22	-0.27931	-2.80315	-1.71161
N23	0.520656	-1.34914	-0.16843
H24	0.479682	-0.97774	0.771849
C25	1.70174	-0.98995	-0.9267
C26	2.762396	-0.517	0.082264
O27	2.474827	-0.25872	1.242545
N28	4.02215	-0.39886	-0.41382
H29	4.19484	-0.70266	-1.35939
C30	5.150739	0.052231	0.395198
H31	5.868829	0.540756	-0.27046
H32	4.790816	0.797387	1.104446
C33	5.834726	-1.08692	1.162582
H34	6.08238	-1.89843	0.459977
H35	5.122349	-1.49083	1.885309
N36	6.989108	-0.56224	1.8945

H37	7.290063	-1.2005	2.621324
H38	7.781278	-0.40224	1.281177
C39	1.412854	0.055867	-2.04697
H40	0.662709	-0.39937	-2.69748
H41	2.320424	0.171585	-2.64791
C42	0.943812	1.410447	-1.56707
C43	1.85113	2.459289	-1.37647
C44	-0.41011	1.646132	-1.30008
C45	1.422397	3.705635	-0.9245
H46	2.903688	2.300827	-1.58862
C47	-0.84224	2.889709	-0.84369
H48	-1.13287	0.85275	-1.45405
C49	0.072867	3.923614	-0.65378
H50	2.14135	4.50576	-0.78632
H51	-1.89482	3.048843	-0.63825
H52	-0.26338	4.892724	-0.30237
H53	2.062973	-1.89446	-1.42796

Item	Value	Threshold	Converged ?
Maximum Force	0.000009	0.00045	YES
RMS Force	0.000002	0.0003	YES
Maximum Displacement	0.001604	0.0018	YES
RMS Displacement	0.000394	0.0012	YES

2.0 Supporting Figures

2.1 Synthetic Scheme

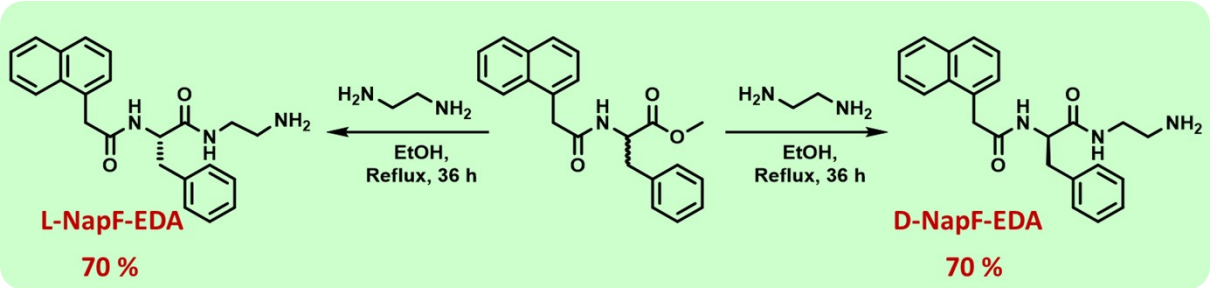

Figure S1: General synthetic scheme of different organic precursors (see section 1.2).

2.2 HT values of NapF-EDA

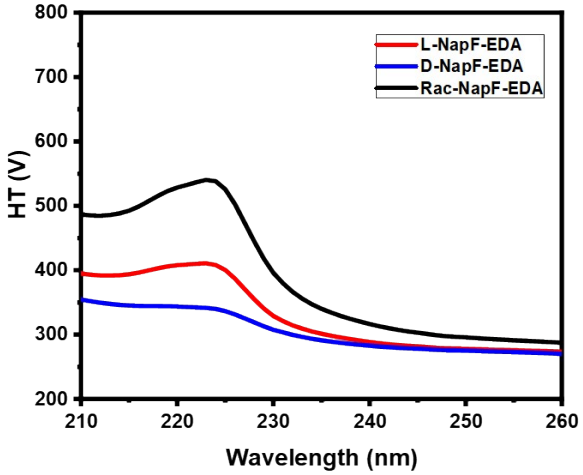

Figure S2: HT values obtained from CD instrument during the collection of CD data reported in Figure 1B. HT values upto 800 V are considered within permissible limits.

2.3 TEM images of self-assembly of PDAs

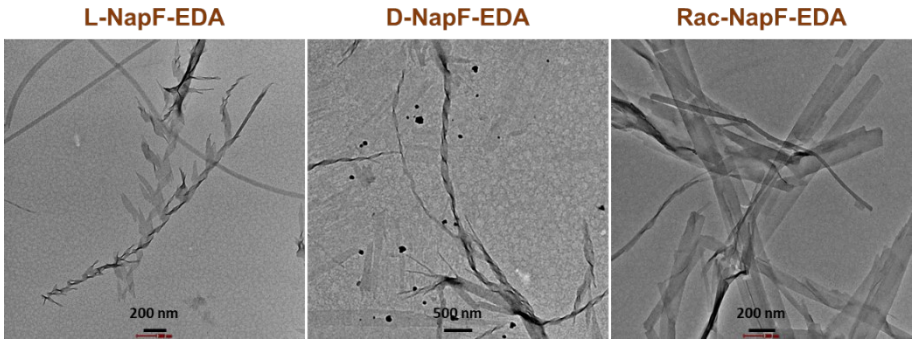

Figure S3: TEM morphology characterization of the self-assemblies formed by L-NapF-EDA, D-NapF-EDA, and their racemic mixture (Rac-NapF-EDA) at pH ~8. The concentration used for the study was 1 mg/mL.

2.4 CD ellipticity values at 298 K for the two enantiomers

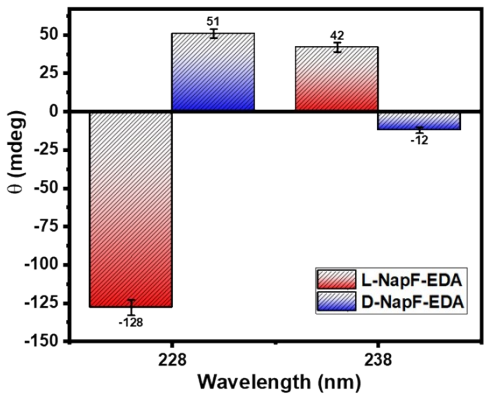

Figure S4: Ellipticity values of L- and D-NapF-EDA at 228 and 238 nm.

2.5 VT CD ellipticity values for the two enantiomers

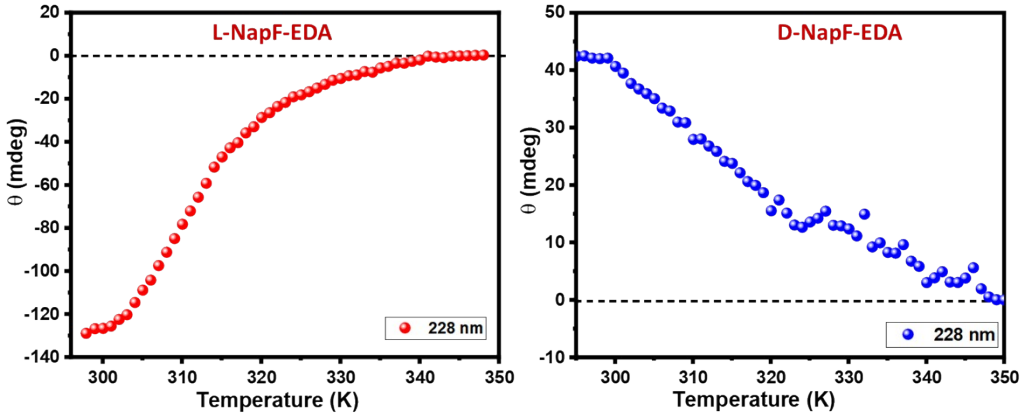

Figure S5: Temperature-dependent ellipticity (mdeg) values of L- and D-NapF-EDA (0.5 mg/mL) at 228 nm for the temperature range 298-348 K.

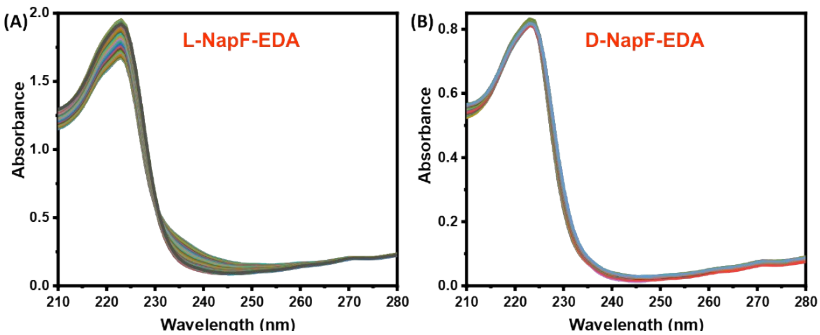

Figure S6: Absorbance data corresponding to the heating profile of both enantiomers (A) L-NapF-EDA and (B) D-NapF-EDA, obtained from CD instrument during the VT CD experiments at 0.5 mg/mL concentration.

2.6 Absorbance plot of VT CD samples

2.7 CD signals of both enantiomers before and after self-assembly

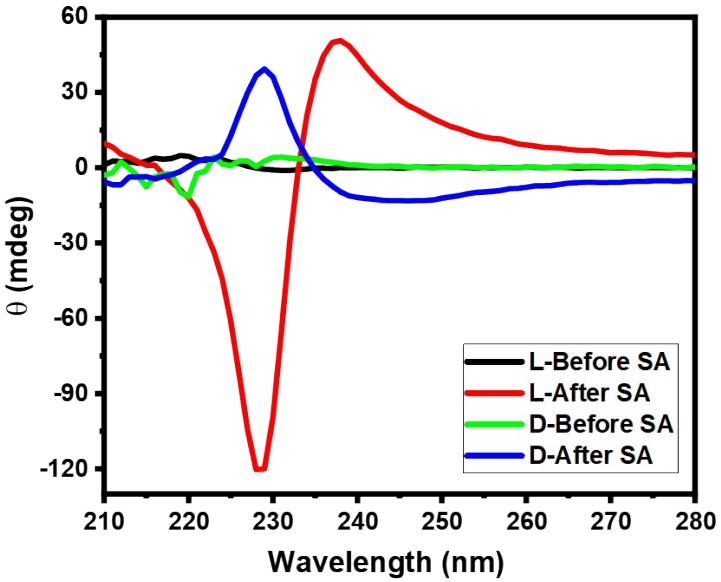

Figure S7: CD signal of both enantiomers before (348 K) and after (298 K) self-assembly formation at a concentration 0.5 mg/mL; SA: Self-assembly.

2.8 pH-responsive reversibility of self-assembly

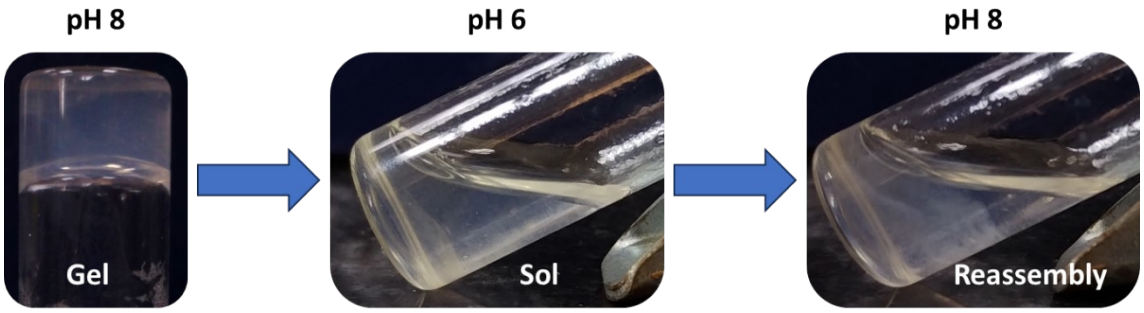

Figure S8: Reversibility of self-assembly formation at acidic and basic pH (concentration 1.5 mg/mL, 4 mM). An increase in turbidity is observed on increasing pH.

2.9 Tyndall effect of NapF-EDA self-assembly

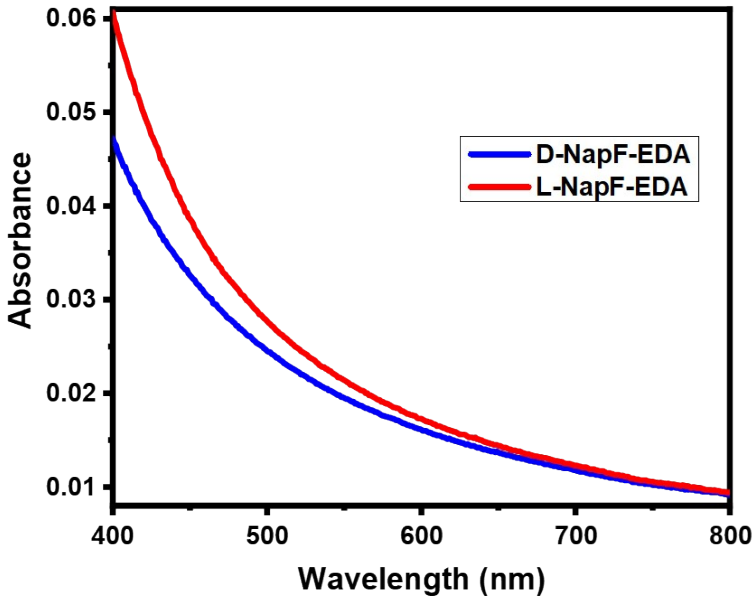

Figure S9: Absorbance of NapF-EDA self-assembly at 600 nm indicating Tyndall effect (concentration 0.3 mg/mL, 0.8 mM).

2.10 pH-responsive Zeta potential of both the enantiomers

Table S1: Zeta potential of both the enantiomers at different pH.

pH	L-NapF-EDA (mV)	D-NapF-EDA (mV)
5	-1.93 ± 0.12	-1.45 ± 0.2
6	0.25 ± 0.1	-0.52 ± 0.05
7	4.78 ± 0.3	0.47 ± 0.13
8	5.88 ± 1.1	4.80 ± 0.5
9	6.10 ± 1	5.32 ± 0.7

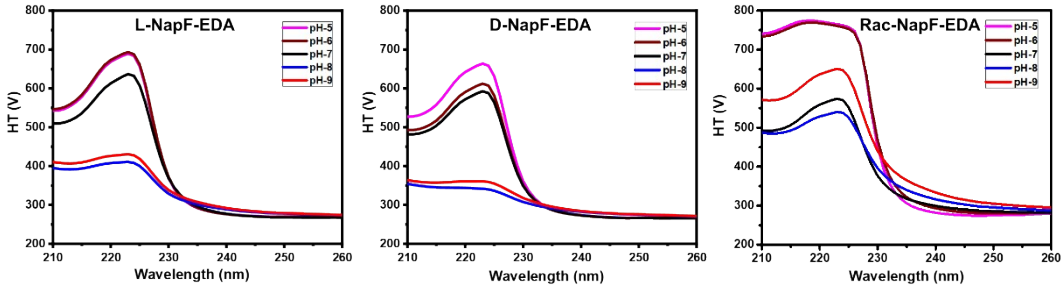

Figure S10: HT values obtained from CD measurement during pH-dependent CD studies (concentration 0.3 mg/mL, 0.8 mM).

2.11 HT values for pH-dependent CD study

2.12 pH-dependent reversible morphology changes

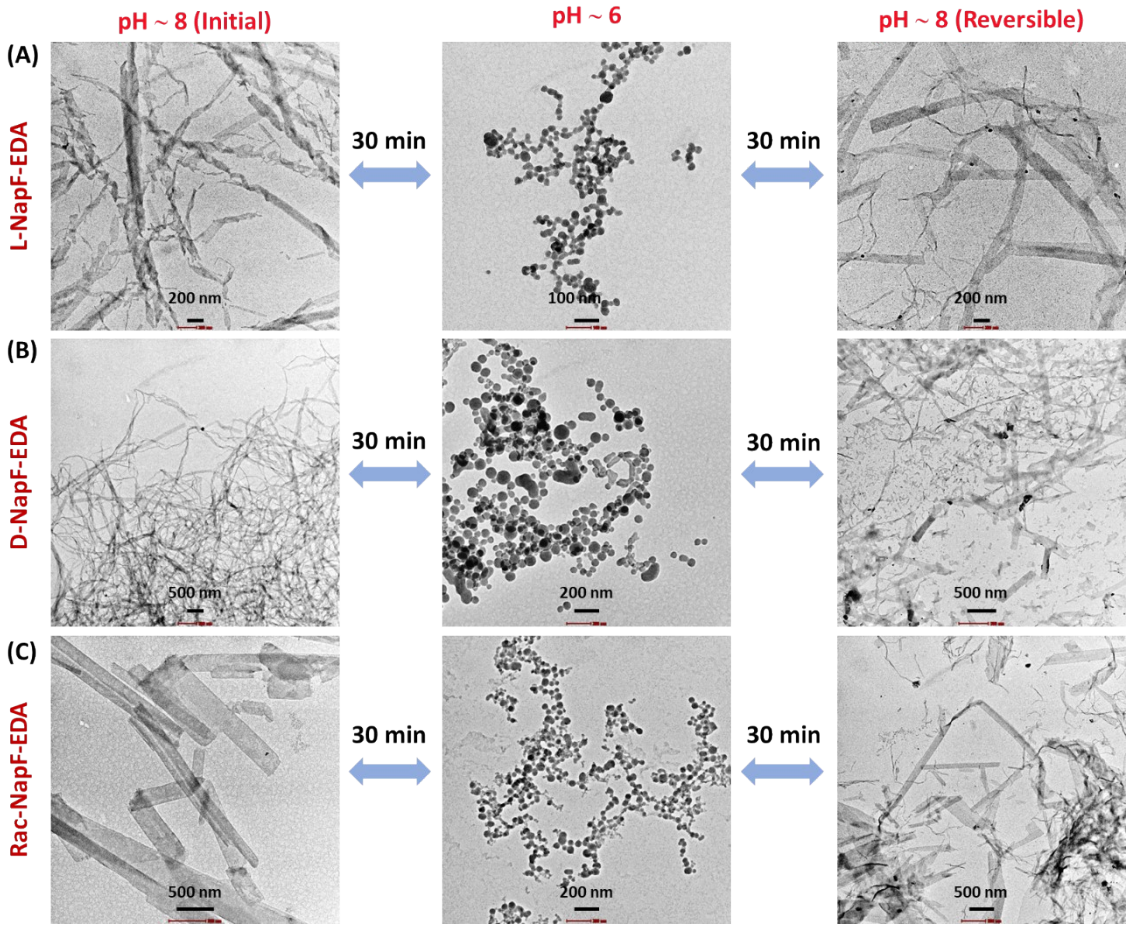

Figure S11: TEM images of pH-dependent reversibility of morphology changes (concentration 0.3 mg/mL, 0.8 mM).

2.13 Summary of differences in the self-assembling behaviour of L- and D-NapF-EDA

Table S2: Differences in various parameters of both the enantiomers.

Parameter	L-NapF-EDA	D-NapF-EDA
Intramolecular interactions	Stronger	Weaker
MGC	Lower (1 mg/mL)	Higher (3 mg/mL)
G' value	Higher (215 Pa)	Lower (40 Pa)
CD signal @298 K, 0.5 mg/mL	Higher (More extent of SA)	Lower (Lesser extent of SA)
Disassembly process	Rapid disassembly (Fast nucleation and Fast elongation)	Slow disassembly (Slow nucleation and Fast elongation)
Re-assembly process	Rapid	Slow
T_m (K)	312 ± 1	317 ± 3
α_T	0.225 ± 0.053	0.4502 ± 0.021
ΔH (kJ mol^{-1})	-125.12 ± 13	-61.24 ± 5
K (M^{-1})	135.2 ± 7	411.7 ± 17
ΔS (J $mol^{-1}K^{-1}$)	-350.2 ± 18	-141.1 ± 10
ΔG (kJ mol^{-1})	-13.055 ± 2	-16.017 ± 2
Hysteresis	Lesser	Larger
Zeta potential (@pH 7)	4.8 mV	0.5 mV

2.14 NMR and Mass data

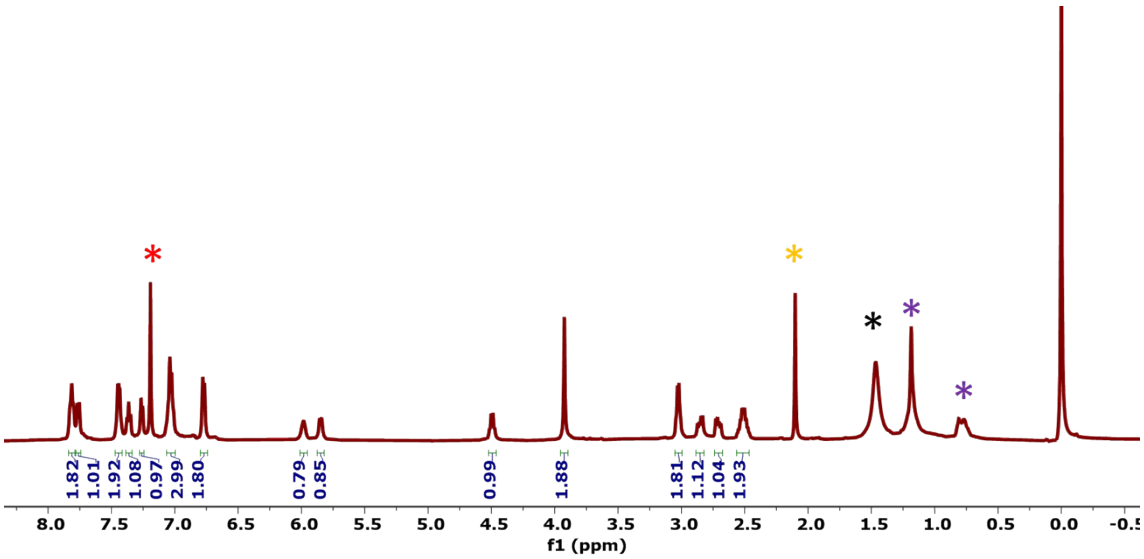

Figure S12: ^{1}H NMR of L-NapF-EDA (500 MHz, $CDCl_3$).

Figure S13: Mass data of L-NapF-EDA.

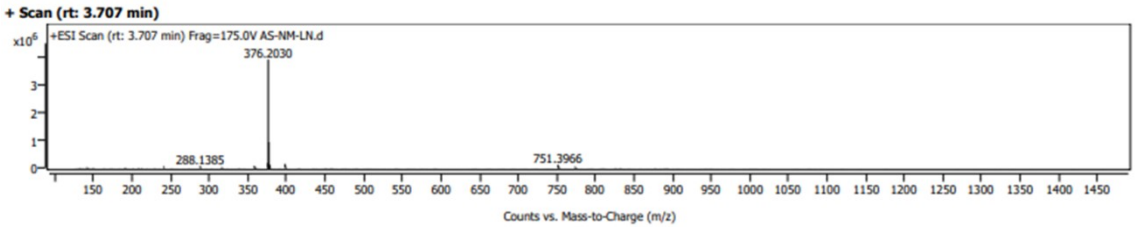

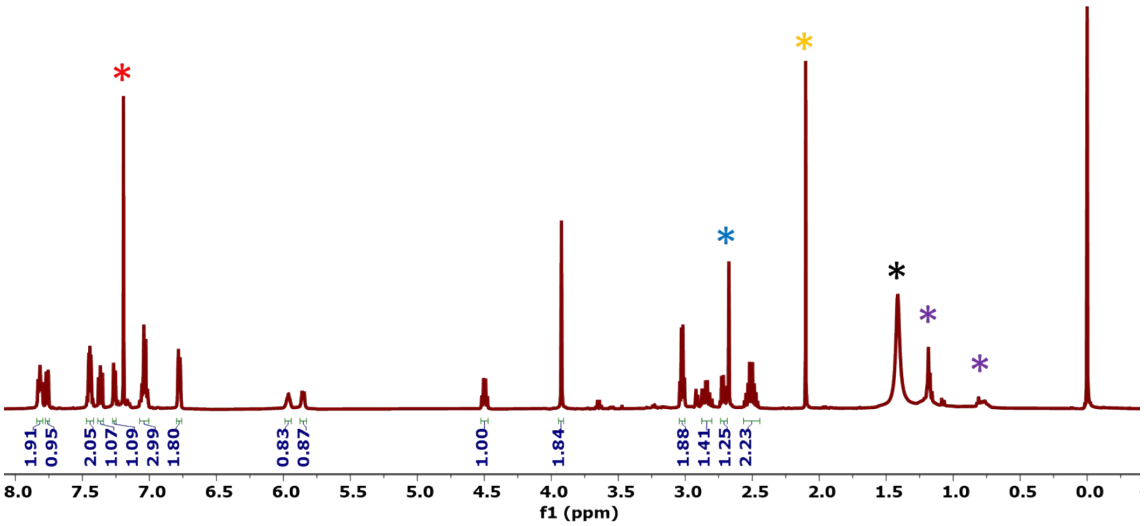

Figure S14: ^{1}H NMR of D-NapF-EDA (500 MHz, $CDCl_3$).

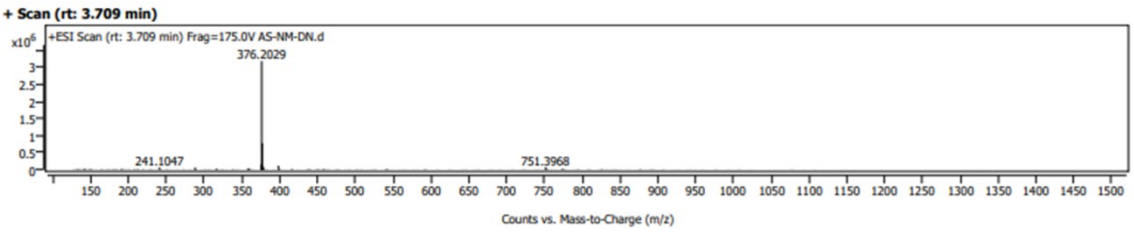

Figure S15: Mass data of D-NapF-EDA.

3.0 References

(1) Reddy, A.; Sharma, A.; Srivastava, A. Optically Transparent Hydrogels from an Auxin–Amino-Acid Conjugate Super Hydrogelator and Its Interactions with an Entrapped Dye. *Chem. – Eur. J.* **2012**, *18* (24), 7575–7581. https://doi.org/10.1002/chem.201103757.

(2) Smulders, M. M. J.; Nieuwenhuizen, M. M. L.; de Greef, T. F. A.; van der Schoot, P.; Schenning, A. P. H. J.; Meijer, E. W. How to Distinguish Isodesmic from Cooperative Supramolecular Polymerisation. *Chem. – Eur. J.* **2010**, *16* (1), 362–367. https://doi.org/10.1002/chem.200902415.

(3) Revision D.01, M. J. Frisch, G. W. Trucks, H. B. Schlegel, G. E. Scuseria, M. A. Robb, J. R. Cheeseman, G. Scalmani, V. Barone, B. Mennucci, G. A. Petersson, H. Nakatsuji, M. Caricato, X. Li, H. P. Hratchian, A. F. Izmaylov, J. Bloino, G. Zheng, J. L. Sonnenberg, M. Hada, M. Ehara, K. Toyota, R. Fukuda, J. Hasegawa, M. Ishida, T. Nakajima, Y. Honda, O. Kitao, H. Nakai, T. Vreven, J. A. Montgomery, Jr., J. E. Peralta, F. Ogliaro, M. Bearpark, J. J. Heyd, E. Brothers, K. N. Kudin, V. N. Staroverov, T. Keith, R. Kobayashi, J. Normand, K. Raghavachari, A. Rendell, J. C. Burant, S. S. Iyengar, J. Tomasi, M. Cossi, N. Rega, J. M. Millam, M. Klene, J. E. Knox, J. B. Cross, V. Bakken, C. Adamo, J. Jaramillo, R. Gomperts, R. E. Stratmann, O. Yazyev, A. J. Austin, R. Cammi, C. Pomelli, J. W. Ochterski, R. L. Martin, K. Morokuma, V. G. Zakrzewski, G. A. Voth, P. Salvador, J. J. Dannenberg, S. Dapprich, A. D. Daniels, O. Farkas, J. B. Foresman, J. V. Ortiz, J. Cioslowski, and D. J. Fox, Gaussian, Inc., Wallingford CT, 2013.